The Journal of Chemical Physics

RESEARCH ARTICLE | JANUARY 07 2025

$TIP4P^{Ice}_{2005}$: Simulating water with two molecular states

Lucía F. Sedano ; Carlos Vega ; Eva G. Noya ; Eduardo Sanz

J. Chem. Phys. 162, 014502 (2025)
https://doi.org/10.1063/5.0247832

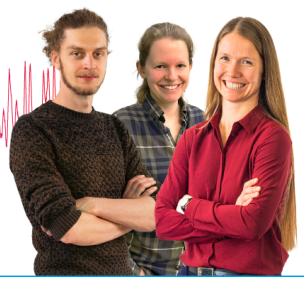

AIP Publishing

The Journal of Chemical Physics ARTICLE pubs.aip.org/aip/jcp

$TIP4P^{Ice}_{2005}$: Simulating water with two molecular states

Cite as: J. Chem. Phys. 162, 014502 (2025); doi: 10.1063/5.0247832
Submitted: 8 November 2024 • Accepted: 17 December 2024 •
Published Online: 7 January 2025

Lucía F. Sedano,[1] Carlos Vega,[1] Eva G. Noya,[2] and Eduardo Sanz[1,a)]

AFFILIATIONS

[1] Departamento de Química Física, Facultad de Ciencias Químicas, Universidad Complutense de Madrid, 28040 Madrid, Spain
[2] Instituto de Química Física Blas Cabrera, CSIC, C/Serrano 119, 28006 Madrid, Spain

[a)] **Author to whom correspondence should be addressed:** esa01@ucm.es

ABSTRACT

Rigid, non-polarizable water models are very efficient from a computational point of view, and some of them have a great ability in predicting experimental properties. There is, however, little room for improvement in simulating water with this strategy, whose main shortcoming is that water molecules do not change their interaction parameters in response to the local molecular landscape. In this work, we propose a novel modeling strategy that involves using two rigid non-polarizable models as states that water molecules can adopt depending on their molecular environment. During the simulation, molecules dynamically transition from one state to another depending on a local order parameter that quantifies some local structural feature. In particular, molecules belonging to low- and high-tetrahedral order environments are represented with the TIP4P/2005 and TIP4P/Ice rigid models, respectively. In this way, the interaction between water molecules is strengthened when they acquire a tetrahedral coordination, which can be viewed as an effective way of introducing polarization effects. We call the resulting model $TIP4P^{Ice}_{2005}$ and show that it outperforms either of the rigid models that build it. This multi-state strategy only slows down simulations by a factor of 1.5 compared to using a standard non-polarizable model and holds great promise for improving simulations of water and aqueous solutions.

I. INTRODUCTION

Water is arguably the most important substance on Earth due to its crucial implications in life. Consequently, water has attracted massive interest from the scientific community. Despite groundbreaking advances in spectroscopic and microscopic techniques,[1,2] a deep understanding of water properties at a molecular scale requires the use of molecular simulations.[3,4]

In this spirit, a good number of classical water models with varying degrees of complexity have been proposed. The most popular ones typically consist of a Lennard-Jones center located on the position of the oxygen, positive charges on the hydrogen atoms, and a negative charge located either at the oxygen as in TIP3P[5] and SPC/E,[6] or at the H–O–H bisector, as in the Bernal–Fowler model,[7] TIP4P family,[5,8–10] and OPC.[11] Finally, some coarse grained models of water (without charges) have also been proposed.[12] It is essential to emphasize that these models differ in their effectiveness at accurately representing the properties of real water.[13,14]

All these water models are rigid and non-polarizable: the geometry of the molecule is fixed (and inspired by that of real water), as are the parameters defining the interaction potential. As a consequence, the dipole moment of each molecule is fixed and does not change with the local environment. This is a major shortcoming because a real water molecule does adapt its electronic structure to the molecular surroundings. In fact, the dipolar moment of water in the liquid phase varies from 2.2 to 3.2 D depending on the local environment, and its value is much higher in the liquid than in the gas phase (i.e., 1.85 D).[15,16]

Flexibility enables some changes in the dipole moment via fluctuations in bond lengths and angles. Consequently, some attempts have been made to introduce this feature in water modeling.[17–19] However, the effect of flexibility is quite small, and flexible models do not significantly improve rigid non-polarizable ones.

A (seemingly) first-principles solution to this problem is to solve Schrodinger's equation on the fly with computer simulations. Since these are costly calculations, typically density functional theory

(DFT) is employed.[20–23] Obviously, in this framework, each water molecule is sensitive, via the electronic density, to the local environment. Until quite recently, testing the predictive ability of DFT was not possible because the calculations were too slow to undertake the computation of thermodynamic properties. However, the upsurge of neural networks[24–26] has enabled tackling relevant problems regarding the phase behavior of water.[4,27–30] Neural network simulations are now only two orders of magnitude slower than empirical force fields (on-the-fly calculations are around 6 orders of magnitude slower). With these technical developments, it has recently been shown that many widely used functionals fail to describe the temperature of maximum density (TMD) or the melting point of ice I_h.[31]

As an alternative to the quantum mechanical approach, there are several means to incorporate the response of molecules to their molecular landscape in classical force fields. One is to introduce vibrations in the position of the partial charges via harmonic oscillators (the so-called Drude models).[32,33] Another approach is to borrow ideas from classical electrostatics and iteratively assign a polarization to each molecule, so that an induced dipole (or even quadrupole) moment is developed in addition to the permanent one. Well-known models of this family are GCPM,[34] AMOEBA,[35] i-AMOEBA,[36] BK3,[37] or HB.[38] Finally, some models, such as the TIP4P-FQ,[39] exploit transfer of charge to confer an environment-responsive character to water molecules. These polarizable force fields are 5–10 times slower than rigid non-polarizable ones, and they do not consistently demonstrate superior predictive accuracy for real water properties.

There is yet another approach to introduce molecular responsiveness denoted as data-driven. The idea is to obtain one, two, three, and four body terms of the potential energy from high level quantum calculations (for instance, coupled cluster) for monomers, dimers, trimers, and tetramers and then add many body effects in the traditional way (i.e., via an electrostatic problem of polarizability leading to an induced dipole moment). Examples of this approach are MB-POL[40,41] and q-AQUA,[42] both following the pioneer work started with the TTM family by Fanourgakis and Xantheas.[43] In general, the latest generation of data-driven models offers a better predictive ability than high-quality rigid, non-polarizable counterparts. However, there is room for improvement.[41] For instance, MB-POL predicts both the melting temperature and the TMD to be around 264 K, in contrast to the experimental values of 273 and 277 K, respectively.[44] Moreover, these models are more than 50 times slower than rigid non-polarizable ones.

In this work, we present a novel strategy to take into account the rearrangement of the electronic distribution of water molecules in response to the local molecular environment. In short, we conceive of water as a mix of two inter-convertible states that transform into each other depending on the local molecular landscape. These states are rigid models. In our case, we combine TIP4P/Ice and TIP4P/2005 to build a model, $\mathrm{TIP4P}^{Ice}_{2005}$, that focuses on the liquid-to-solid transition. The molecular environment is quantified with a local bond order parameter that is sensitive to the degree of ice-like order[45] (it has recently been shown that the dipole moment of water correlates quite well with certain local order parameters[46–48]). In our scheme, molecules in a more tetrahedral local environment acquire TIP4P/Ice parameters, becoming more polar than molecules in a looser order environment, which are represented by TIP4P/2005. With our approach, which resembles the idea of conceiving water as a mix of two molecular structures,[30,49–56] we are able to improve the representation of water provided by either TIP4P/Ice or TIP4P/2005 at the sole cost of slowing down the simulations by less than a factor of two.

This work serves as a proof of concept for a new modeling strategy that effectively incorporates polarizability in a simple and efficient way. We do not claim that $\mathrm{TIP4P}^{Ice}_{2005}$ is superior to other well-established polarizable models. We simply present this idea as a proof of concept and leave the exploration of the formalism's limits (through the use of other appropriate order parameters, an increased number of molecular internal states beyond two, and the exploration of other water models as representative states) to future work.

Our approach could also open interesting avenues in the simulation of other systems, such as aqueous electrolyte solutions, many of whose properties are not satisfactorily captured[57] by non-polarizable force fields.[58,59] Even models with rescaled charges[60–66] or polarizable ones[67–70] struggle in comprehensively describing the dynamic and thermodynamic behavior of real aqueous solutions. It may be worth exploring in the future whether our strategy leads to significant improvements in the modeling performance of ionic solutions.

II. APPROACH AND HAMILTONIAN

Real molecules alter their structure in response to the interaction with other surrounding molecules. This rearrangement is neglected in simulations using non-polarizable models. The main idea of our approach is to dynamically assign a non-polarizable model to each molecule depending on its local molecular environment.

We will illustrate our approach with two consolidated water models: TIP4P/2005[9] and TIP4P/Ice.[10] Both models have very similar geometries (see Sec. IV). TIP4P/2005 accurately predicts liquid water properties,[13] whereas TIP4P/Ice works very well for ice phases.[13,71] Consequently, if a molecule finds itself in a low-order, liquid-like molecular environment, we model it with TIP4P/2005, whereas for high-order ice-like environments, the TIP4P/Ice model is used. The model assignment is dynamical along the simulation: when a molecule changes its environment, it switches from one model/state to another.

In this work, we use the $\bar{q}_6$ local-bond order parameter[45] (computed with a cutoff radius of 3.5 Å), which assigns a scalar to every molecule depending on its local environment, to discriminate between low and high local order. Only oxygen atoms are considered for the calculation of $\bar{q}_6$. The threshold value, $\bar{q}_{6,t}$, chosen to discriminate between high order ($\bar{q}_6 > \bar{q}_{6,t}$) and low order ($\bar{q}_6 \leq \bar{q}_{6,t}$) environments, is $\bar{q}_{6,t} = 0.25$. This value has been optimized to predict several target properties (see Appendix B).

The order parameter that dictates the transition between molecular states is part of the model's Hamiltonian. $\bar{q}_6$ has proven very effective in discriminating liquid from solid-like environments in water,[45,72,73] and we chose it because of our interest in the liquid-to-solid transition.[71,74,75] In Sec. V, we mention alternative order parameters that could be employed in the future within the simulation scheme we propose in this article.

The cross-interaction between TIP4P/2005 and TIP4P/Ice molecules obeys the Coulomb law for the interaction between

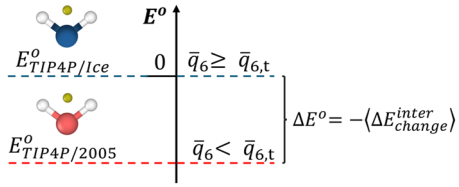

FIG. 1. Sketch of our TMS water model, where molecules change from TIP4P/Ice to TIP4P/2005 (or vice versa) depending on their $\bar{q}_6$ value. The energy difference between both states, ΔE^0, is approximated by minus the average inter-molecular energy change upon identity switches, $\langle -\Delta E^{inter}_{change} \rangle$ (see Sec. VII).

charges and the Lorentz–Berthelot combination rules for the Lennard-Jones interaction parameters. We name our two molecular states model (TMS) that combines two different rigid water potentials as $\text{TIP4P}^{Ice}_{2005}$.

In the combined model of water, we have to take into account that the potential energy of a water molecule in the TIP4P/2005 "state," $E^0_{TIP4P/2005}$, is different from that in the TIP4P/Ice "state," $E^0_{TIP4P/Ice}$. We discuss in Sec. VII the values of these intra-molecular potential energies. In Fig. 1, we sketch the Hamiltonian of our TMS model.

III. SIMULATION SCHEME

Rigorously, every time a molecule changes position, its $\bar{q}_6$ should be evaluated to check if it crosses $\bar{q}_{6,t}$. In a Monte Carlo scheme, this would be easy to implement: whenever a trial move for a given molecule is considered, $\bar{q}_6$ is evaluated, and the state assignment is made accordingly. However, simulating water with Monte Carlo is extremely inefficient from a computational point of view.

For the sake of efficiency, we do a sequence of short molecular dynamics trajectories and update the molecular states at the end of each trajectory. The simulation scheme is as follows: (i) a short molecular dynamics trajectory of duration τ_{smd} is run; (ii) $\bar{q}_6$ is computed for each water molecule at the end of this short run; (iii) the TIP4P/Ice model is assigned to molecules with $\bar{q}_6 > \bar{q}_{6,t}$, and the TIP4P/2005 model is assigned to the rest of the molecules; (iv) step i is repeated again, starting the new trajectory with the final positions and velocities of the previous one.

In this scheme, $\bar{q}_{6,t}$ is a parameter of the model; hence, the thermodynamic properties of $\text{TIP4P}^{Ice}_{2005}$ are conditioned by the specific choice of $\bar{q}_{6,t}$. In Appendix B, we show that $\bar{q}_{6,t} = 0.25$ provides good results in comparison to other threshold choices. On the other hand, τ_{smd} has to be small enough in order to avoid structural rearrangements along the short trajectory but long enough to maintain computational efficiency. In Sec. VIII, we discuss the choice of τ_{smd}. The main body of results of this paper was obtained with $\tau_{smd} = 10$ ps.

IV. SIMULATION DETAILS

The two models used throughout this work (TIP4P/2005[9] and TIP4P/Ice[10]) have the same bond distances and angles so that the positions of the O and H atoms do not change upon state transitions (although the position of the negatively charged *M* center, which is located along the molecule bisector, does change). The models differ in the value of the point charges (a certain positive charge on each hydrogen and a negative one, of double absolute value, located on the *M* site) and in the Lennard-Jones parameters of the oxygen atom.

All simulations were carried out using the GROMACS 4.6.7 software[76] with a molecular dynamics time step of 2 fs. Pressure and temperature were fixed with a Parrinello–Rahman barostat[77] (isotropic for the liquid phase and anisotropic for the solid phase and the coexistence simulations) and a Nose–Hoover thermostat,[78,79] respectively, both with a coupling constant of 2 ps. The cutoff was set to 9 Å for dispersive and Coulombic forces. Standard Lennard-Jones corrections were included[80] (also for direct coexistence[81,82] simulations). The particle mesh Ewald method[83,84] was employed for the long-ranged electrostatic interactions. The LINCS algorithm[85] constrained the molecules' geometry during the simulations. For bulk simulations, systems containing 432 molecules were studied in the *NpT* ensemble. For the direct coexistence simulations, systems of 4000 water molecules were studied (a system size for which the uncertainty of the melting point is about two Celsius degrees[86]); half of these molecules were in the liquid state, while the other half were in the solid state, exposing the secondary prismatic plane of ice I_h at the interface.

In order to evaluate the free energy of the solid, we used the Einstein molecule method.[87,88] Unless otherwise stated, all the simulation details are the same as previously described. Previous *NpT* simulations at the thermodynamic states of interest were performed to obtain the equilibrium density and lattice constants. Knowing these parameters, a perfect solid was generated implementing the algorithm proposed by Buch *et al.* for the proton disorder.[89] The states under consideration were 1 bar at the temperatures of 250 and 270 K (i.e., the melting temperatures of the potential models used in this work), and the system consisted of 432 molecules. The velocity rescaling thermostat proposed by Bussi *et al.* was employed with a coupling of 2 ps. For computing the term ΔA_1, which corresponds to the free-energy difference between the ideal Einstein crystal and the Einstein crystal in which molecules interact through the Hamiltonian of the real solid ("interacting" Einstein crystal), *NVT* simulations were carried out with a time step of 1 fs, and configurations were saved every 100 steps from a trajectory of 1 ns, where each atom is an ideal gas particle attached to its lattice position by a harmonic spring. The energy of these instantaneous configurations is then evaluated through the interacting potential and compared to that of the ideal lattice. This energy difference must be of the order of 0.002–0.004 Nk_BT, which can be controlled by fixing the value of the harmonic spring constant Λ_E. For this particular case, the maximum value (Λ_E) was determined to be 5000 $k_BT/$ Å^2. In the next step, different values of the spring constant, Λ_E', are simulated for 5 ns, ranging from 0 (no interaction) to the previously established value of Λ_E (maximum interaction) in order to obtain, via thermodynamic integration, the energy difference between the interacting Einstein crystal and the solid of interest (ΔA_2). The numerical integration is performed by selecting 16 values of Λ_E' for the Gauss–Legendre quadrature algorithm.[90]

Finally, the term A_0 is computed from the partition function of the ideal Einstein crystal using Monte Carlo integration[80] with a narrowed-down sampling around the maximum displacement and rotation, which are determined from a short simulation. 10^9 MC

steps were used to evaluate these integrals. For further details on the Einstein molecule methodology, we refer the reader to Refs. 87, 88, and 91.

V. BULK PROPERTIES

In Fig. 2, we show the distribution of $\tilde{q}_6$ values taken by the molecules of a bulk liquid (in orange) and a bulk ice I_h solid (in green) simulated with the TIP4P$^{Ice}_{2005}$ model at 250 K and 1 bar. The vertical line indicates the threshold value ($\tilde{q}_{6,t}$ = 0.25) above which molecules are assigned the TIP4P/Ice parameters. The main idea we want to highlight from Fig. 2 is that all molecules in the solid are in the TIP4P/Ice state (whereas in the liquid more than half of the molecules are TIP4P/2005). In Fig. 3, we plot the fraction of molecules in the TIP4P/Ice state, $X_{TIP4P/Ice}$, as a function of temperature for the liquid phase at 1 bar. Such fraction is a state function that decreases with temperature due to the loss of structural order in the liquid. We note that the composition around ambient temperature is similar to the high- to low-density ratio inferred from experiments.[92,93]

In Fig. 4(a), the density–temperature dependence of the liquid at 1 bar is displayed for the TIP4P$^{Ice}_{2005}$ model (purple curve) as compared to those of the TIP4P/Ice (blue curve) and the TIP4P/2005 (red curve) models. The density of the TMS model lies in between those of the single-state models. In part (b) of the same figure, we show the temperature dependence of the enthalpy of the TSM and the single-state models (with the same color code as that used for the density). Again, the energy of the TIP4P$^{Ice}_{2005}$ model lies in between those of the single-state models.

We now check if the properties of TIP4P$^{Ice}_{2005}$ can be approximated as if it were an ideal mix (*idmix*) composed of TIP4P/Ice and TIP4P/2005 via

$$\Phi_{idmix} = \Phi_{TIP4P/2005} X_{TIP4P/2005} + \Phi_{TIP4P/Ice} X_{TIP4P/Ice}, \quad (1)$$

where Φ is a generic thermodynamic property (density, internal energy, etc.). In fact, using this molar-fraction-weighted

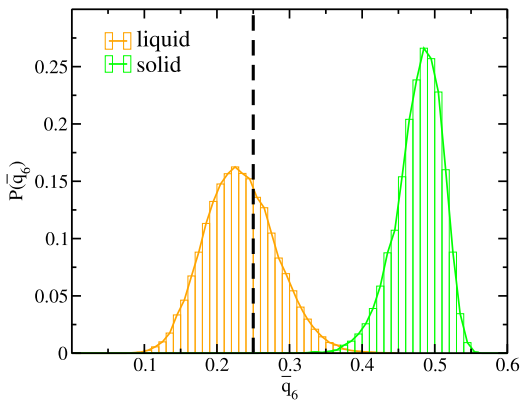

FIG. 2. Normalized $\tilde{q}_6$ histogram for the TIP4P$^{Ice}_{2005}$ liquid (orange) and solid (green) phases at 250 K and 1 bar. The dashed vertical line corresponds to the threshold ($\tilde{q}_{6,t}$) that sets the transition between the TIP4P/2005 and the TIP4P/Ice states.

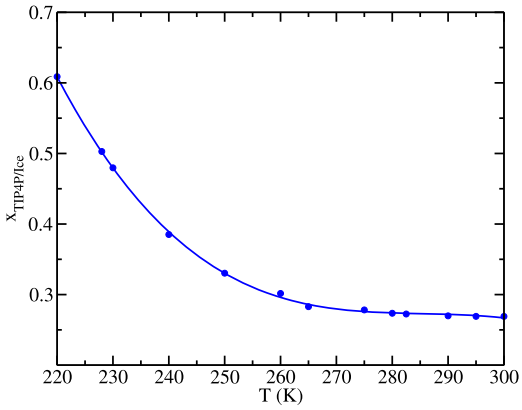

FIG. 3. Fraction of TIP4P/Ice particles ($X_{TIP4P/Ice}$) in the TIP4P$^{Ice}_{2005}$ model as a function of temperature for the liquid phase (at 1 bar). Circles are simulation points, and the solid line is a cubic fit for visual guidance.

combination, one virtually recovers the density and the energy of TIP4P$^{Ice}_{2005}$ from the corresponding properties of the single state models (purple diamonds in Fig. 4).

One may be tempted to think that it is not worth simulating the TMS model in view of the fact that its properties can be predicted through an ideal mix of the single-state models. First of all, to apply the ideal mixing rule, one first needs to run TMS model

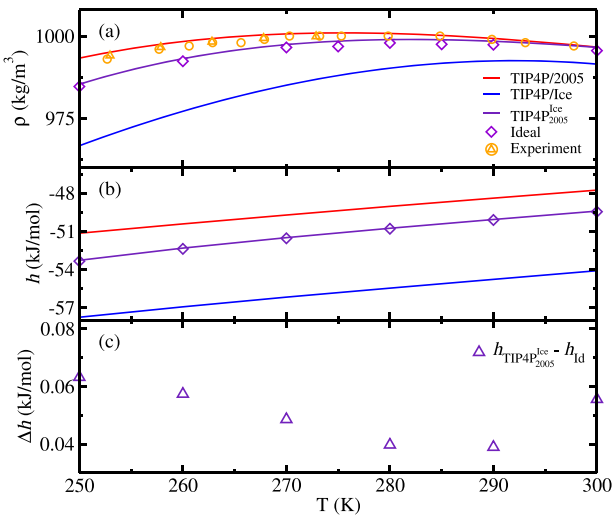

FIG. 4. Thermodynamic properties as a function of temperature for TIP4P/Ice, TIP4P/2005, and TIP4P$^{Ice}_{2005}$, and for an ideal mixing of the single-state models [following Eq. (1)] as indicated in the legend. (a) Density. Solid lines are cubic fits to the simulation data. Experimental results are taken from Ref. 106 (triangles) and Ref. 107 (circles). (b) Molar enthalpy. (c) Molar enthalpy difference between that of TIP4P$^{Ice}_{2005}$ and the enthalpy obtained assuming an ideal mix of the single-state components [Eq. (1)]. The kinetic term of the enthalpy (which is 3*RT* for all models, *R* being the ideal gas constant) has not been included in the graphs.

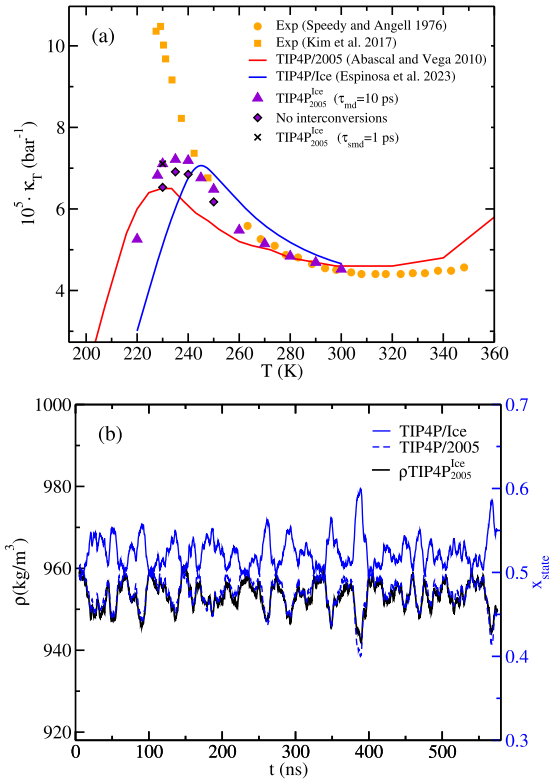

FIG. 5. (a) Isothermal compressibility at 1 bar as a function of temperature for several models and experiments as indicated in the legend. In this work, we performed the simulations for the TIP4P$^{Ice}_{2005}$ model. At low temperatures, runs as long as 580 ns were required to reach convergence. (b) Averaged density every 10 ns (black line) and composition (blue lines) vs time for the TIP4P$^{Ice}_{2005}$ model at 230 K [near the compressibility maximum shown in part (a)].

simulations to get the molar fraction, which is a state function (Fig. 3). In addition, there are small but systematic and noticeable differences between the TIP4P$^{Ice}_{2005}$ model and the ideal mix combination of the TIP4P/Ice and TIP4P/2005 models. Actually, the enthalpy of the TMS model is slightly larger than that of the individual models ideally combined [see the enthalpy difference in Fig. 4(c)].

Moreover, the thermodynamic properties of the TMS model are not always comprised between those of the single-state models. In fact, the isothermal compressibility, κ_T, of the TIP4P$^{Ice}_{2005}$ model [purple triangles in Fig. 5(a)], reaches a maximum that is larger than either κ_T maxima of the single-state models (blue and red lines for the TIP4P/Ice and TIP4P/2005 models, respectively). The increase of κ_T on cooling is a water anomaly[94] that, from a thermodynamic point of view, is related to the slope of the temperature of maximum density curve in the (p, T) plane.[95] Structurally, the rise of compressibility when temperature decreases is supposedly due to the emergence of liquid domains with different densities[96] (structural heterogeneities enhance volume fluctuations and, hence, the compressibility[97]).

It is then quite tempting to hypothesize that the accentuation of compressibility when going from single-state models to the TIP4P$^{Ice}_{2005}$ model is due to the concomitance between density and identity fluctuations. To assess this hypothesis, we plot in Fig. 5(b) the density and the molar fraction of each state over time for a TIP4P$^{Ice}_{2005}$ liquid close to the compressibility maximum (230 K). Such a liquid displays an almost equi-molar composition (see Fig. 3) which, again, suggests that composition heterogeneity enhances compressibility. Clearly, low-density fluctuations are correlated with an increase of the TIP4P/Ice state population (and high-density ones are accompanied by a raise of the TIP4P/2005 content). This correlation accentuates density fluctuations given that the density of the TIP4P/Ice liquid is lower than that of TIP4P/2005 [see Fig. 4(a)].

We get further support of the correlation between composition and density by running, for a few temperatures, simulations of the liquid with the corresponding average population but not allowing for interconversion between states. The expectation is that κ_T will decrease when there are no inter-conversions because density fluctuations cannot be accentuated by composition fluctuations. This is in fact what is seen in Fig. 5, with diamonds (no interconversions) lying systematically below triangles (interconversions) at low temperatures.

In Ref. 96, it is argued that, since κ_T is proportional to volume fluctuations, its maximum must correspond to an equal population of high- and low-density liquid domains.[96] In our case, the κ_T maximum corresponds to a similar population of TIP4P/Ice and TIP4P/2005 states. This parallelism, however, should not be interpreted as if half of the system was low-density liquid composed of TIP4P/Ice molecules and the other half high-density liquid composed of TIP4P/2005 molecules. The reason why such an interpretation is too simplistic is that $\bar{q}_6$ is not devised for distinguishing between molecules belonging to high- and low-density liquid domains. More recent and sophisticated order parameters[54,98–103] are required for that purpose. In this work, we use $\bar{q}_6$ because we are mainly interested in the liquid-to-solid transition, but it is certainly worth applying our approach in combination with an order parameter that identifies the liquid density domain to which water molecules belong in order to focus on the physics of supercooled water.

The fact that TIP4P$^{Ice}_{2005}$ enhances the compressibility can be exploited to improve water modeling. Non-polarizable water models typically underestimate the experimental compressibility at low temperatures[104,105] [see, e.g., the comparison between TIP4P/Ice (blue), TIP4P/2005 (red), and experimental data (orange) in Fig. 5]. The compressibility enhancement induced by TIP4P$^{Ice}_{2005}$ goes in the right direction, but it is not enough. One should take into account that the $\bar{q}_6$ order parameter we use in this work is not tailored to distinguish high-density from low-density liquid regions, as previously discussed.

In summary, bulk liquid properties of the TMS model such as the density or the internal energy are well approximated by an ideal mixing combination of the single state models (even though there are small systematic differences between the internal energy of the TIP4P$^{Ice}_{2005}$ and the combination between those of TIP4P/Ice and TIP4P/2005). The compressibility of the TMS model at low temperatures, however, is not intermediate between those of the single state models. Instead, it is larger than the compressibility of either

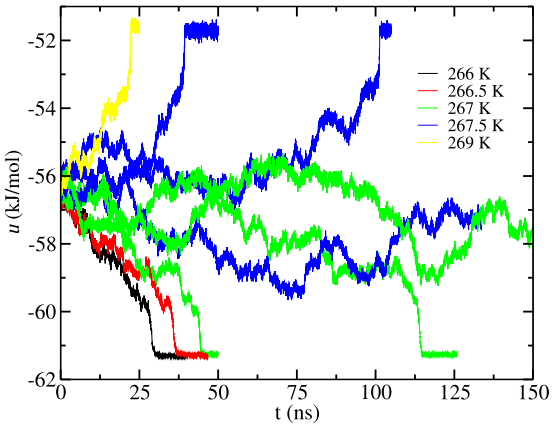

FIG. 6. Potential energy per mol vs time for the TIP4P$^{Ice}_{2005}$ model at different temperatures (see legend) and 1 bar starting from a configuration of ice I_h in contact with liquid water.

single state model due to correlations between state identity and density.

VI. MELTING TEMPERATURE

To determine the melting temperature, we perform direct coexistence simulations[108,109] at constant pressure (1 bar) and different temperatures. These simulations start from a configuration where half of the box is ice I_h and the other half is liquid water. For temperatures below melting, ice grows, and vice versa. To determine whether ice grows or melts, we monitor the potential energy, which goes down along the trajectory if ice grows (and vice versa). In Fig. 6, we plot the molar potential energy vs time for several trajectories at different temperatures. From these simulations, we infer that the melting temperature of the TMS model is $T_m = 267.5 \pm 2$ K.

The computed T_m lies between those of the single-state models (250 and 270 K for TIP4P/2005[110–112] and TIP4P/Ice, respectively), although it is closer to that of TIP4P/Ice. In the TIP4P$^{Ice}_{2005}$ model, TIP4P/2005 molecules become TIP4P/Ice as they incorporate into the solid in response to the ordered local environment. This state change strengthens the interaction with other ice molecules and favors the ice phase with respect to the case in which molecules always remain in a single-state TIP4P/2005 model. This state change intends to mimic the process by which real water molecules rearrange their electronic structure to establish more favorable interactions with the surrounding molecules (for instance, the dipolar moment increases by 60% when going from the vapor to the liquid phase[15,16]).

In general, the TMS Hamiltonian can improve the modeling of water whenever there are marked structural heterogeneities across the system. Other than solid–liquid direct coexistence, examples of heterogeneous distribution of local order throughout the simulation box are crystal nucleation, where crystal nuclei embedded in the liquid are simulated,[4,71,75] or simulations of deeply supercooled water, where structural heterogeneities are expected to be enhanced due to the appearance of interpenetrated low density ordered regions and high density disordered ones.[53,56,96]

VII. INTRA-MOLECULAR ENERGY AND MELTING ENTHALPY

The energy of a given phase (liquid or solid) is given by

$$E_{phase} = E^{inter}_{phase} + X_{TIP4P/2005} E^0_{TIP4P/2005} + X_{TIP4P/Ice} E^0_{TIP4P/Ice}. \quad (2)$$

Where the first term in the right hand side accounts for the inter-molecular interactions and the others for the intra-molecular potential energy associated with the states in which a given water molecule can be found (see Fig. 1). Since we are interested in energy differences between different phases rather than in absolute energies, we can arbitrarily set the energy associated with one of the states as the reference intra-molecular energy. For convenience, we chose $E^0_{TIP4P/Ice} = 0$, given that all molecules in the solid phase are in the TIP4P/Ice state ($X_{TIP4P/2005} = 0$; see Fig. 2). Then, the energy of the solid phase is simply given by

$$E_{solid} = E^{inter}_{solid}, \quad (3)$$

whereas that of the liquid is given by

$$E_{liquid} = E^{inter}_{liquid} + X_{TIP4P/2005} \Delta E^0_{Ice-2005}, \quad (4)$$

where $\Delta E^0_{Ice-2005}$ is $E^0_{TIP4P/2005} - E^0_{TIP4P/Ice}$.

The question now is what value does $\Delta E^0_{Ice-2005}$ take. According to our Hamiltonian (Sec. II), every particle that crosses the $\tilde{q}_6$ threshold ($\tilde{q}_{6,t} = 0.25$) must change its identity. An identity change is accompanied by a change of inter-molecular interactions. This inter-molecular energy change upon identity change, $\Delta E^{inter}_{change}$, must be compensated by an equal change of opposite sign of intra-molecular energy. Otherwise, there would be a net gain/loss of energy after identity changes. To better understand this, let us think of the possibility of running our TMS Hamiltonian with Monte Carlo. The only way to ensure acceptance of all identity changes—as we do in our molecular dynamics scheme—is to compensate the associated inter-molecular energy change with an opposite intra-molecular energy change. Therefore, $\Delta E^0_{Ice-2005}$ can be approximated by $-\langle \Delta E^{inter}_{change} \rangle$, the average inter-molecular potential energy change when a molecule changes identity from TIP4P/Ice to TIP4P/2005 (with the opposite sign). Such inter-molecular energy change is positive because the charges in the TIP4P/2005 model are lower than in TIP4P/Ice. Consequently, $\Delta E^0_{Ice-2005}$ is negative. In other words, the intra-molecular energy of the TIP4P/2005 state of water is lower than that of the TIP4P/Ice state. These energy levels are sketched in Fig. 1.

In practice, to estimate $\Delta E^0_{Ice-2005}$, we identify in TIP4P$^{Ice}_{2005}$ liquid configurations the TIP4P/Ice molecules that are on the verge of crossing the $\tilde{q}_6$ threshold, change their identity, and compute the associated average inter-molecular potential change (and change its sign). In Fig. 7, we plot the estimate of $\Delta E^0_{Ice-2005}$ thus obtained as a function of temperature (up triangles). We can also identify TIP4P/2005 molecules on the verge of crossing the threshold, change their identity to TIP4P/Ice, and obtain another estimate of $\Delta E^0_{Ice-2005}$ through the associated average inter-molecular energy change (with no sign change in this case; down triangles in Fig. 7). Both strategies yield estimates of $\Delta E^0_{Ice-2005}$ close to each other, with small systematic differences due to the fact that the molecules belonging

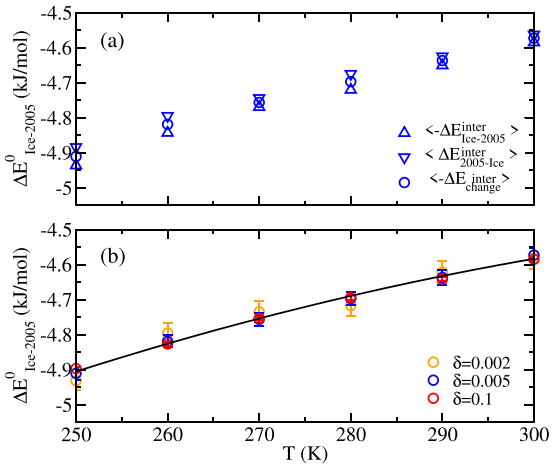

FIG. 7. Estimates of $\Delta E^0_{Ice-2005}$ (per mol) as a function of temperature. (a) Up-triangles represent the average inter-molecular energy variation (with opposite sign) associated with an identity change from TIP4P/Ice to TIP4P/2005 for δ = 0.005, whereas down-triangles correspond to the reverse identity change (with no sign change). The mean value of $\Delta E^0_{Ice-2005}$ is represented by circles. (b) Same as circles in (a) but for different values of δ (see legend). The solid line is a quadratic fit to all the data.

to the selected set for the calculation have slightly different molecular environments. More specifically, TIP4P/Ice molecules have a $\bar{q}_6$ comprised between 0.25 and 0.25+δ, whereas TIP4P/2005 ones have $\bar{q}_6$ values between 0.25−δ and 0.25, where δ is half of the width of the window used to identify molecules on the verge of crossing $\bar{q}_{6,t}$. In Fig. 7(a), we have used δ = 0.005. Although the difference between TIP4P/Ice-TIP4P/2005 (up triangles) and TIP4P/2005-TIP4P/Ice (down triangles) transformations depends slightly on δ, the average value [circles in Fig. 7(a)] does not. This is shown in Fig. 7(b), where we plot the average $\Delta E^0_{Ice-2005}$ as a function of temperature for several values of δ. We get $\Delta E^0_{Ice-2005}$ at any temperature through a fit to the data in Fig. 7(b). In Sec. IX, we show that obtaining $\Delta E^0_{Ice-2005}$ as described earlier makes T_m calculations through free energy calculations of bulk phases separately fully consistent with direct coexistence simulations. This consistency strongly supports the validity of our definition and computation of $\Delta E^0_{Ice-2005}$.

Once we have $\Delta E^0_{Ice-2005}$, and using Eqs. (3) and (4), it is straightforward to compute the melting enthalpy, ΔH_m,

$$\Delta H_m = E_{liquid,m} - E_{solid,m} + \Delta(pV)_m, \tag{5}$$

where $\Delta(pV)_m$ is the pV difference upon melting (which is a small contribution at 1 bar). The melting enthalpy of the TIP4P$^{Ice}_{2005}$ model is reported, alongside that of the single-state models, in Table I. The TIP4P$^{Ice}_{2005}$ melting enthalpy (at 267.5 K) is 1.47 kcal/mol, which is very close to the 1.44 kcal/mol of real water. The melting enthalpies of the single-state models, in contrast, underestimate the real value by 15%–20% (1.13 and 1.20 kcal/mol for TIP4P/2005 and TIP4P/Ice, respectively).

To better understand the melting enthalpy of the TMS model, we split it into an inter-molecular and an intra-molecular term,

$$\Delta H_m = \Delta H^{inter}_m + X_{TIP4P/2005}\Delta E^0_{Ice-2005}. \tag{6}$$

The inter-molecular term ΔH^{inter}_m [which is equal to $E^{inter}_{liquid} - E^{inter}_{solid} + \Delta(pV)_m$] is 2.29 kcal/mol, which is significantly larger than the melting enthalpy of either single-state model. The inter-molecular enthalpy is enhanced because the point charges of the TIP4P/Ice model are about 6% larger than those of TIP4P/2005 [recall that all ice molecules are in the TIP4P/Ice state, whereas the liquid ones are mainly TIP4P/2005 (about 70% at T_m, according to Fig. 3)]. However, the inter-molecular term is compensated by a negative intra-molecular melting energy ($X_{TIP4P/2005}\Delta E^0_{Ice-2005}$ = −0.82 kcal/mol), resulting in a melting enthalpy that lies within 2% of the experimental value (see Table I).

VIII. TUNING τ_{smd}

The simulation time of each short molecular dynamics trajectory, τ_{smd}, is a parameter that needs to be properly tuned. Rigorously, our Hamiltonian would require that the identity of the molecules is updated every molecular dynamics step. However, this would dramatically slow down the simulation, as the fraction of time spent

TABLE I. Selected thermodynamic properties of the TIP4P$^{Ice}_{2005}$ model compared to those of its constituent models (TIP4P/Ice and TIP4P/2005) and to that of real water. TMD stands for *temperature of maximum density*. The subscripts *m*, *liq*, and *sol* stand for *melting*, *liquid*, and *solid*, respectively.

	Expt.	TIP4P/2005		TIP4P/Ice		TIP4P$^{Ice}_{2005}$	
Property	Value	Value	%Dev.	Value	%Dev.	Value	%Dev.
TMD (K)	277	277.3	0	294	6	282.9	2
T_m (K)	273.15	250	−8	270	−1	267.5	−2
TMD-T_m (K)	3.90	27.3	610	24.0	520	15.4	300
ΔH_m (kcal/mol)	1.44	1.13	−22	1.20	−17	1.47	2
$\rho_{298K,liq}$ (g/cm^3)	0.999	0.997	−0.2	0.992	−0.7	0.997	−0.2
$\rho_{m,liq}$ (g/cm^3)	0.997	0.994	−0.3	0.985	−1.2	0.996	0.2
$\rho_{m,sol}$ (g/cm^3)	0.917	0.921	0.4	0.906	−1.2	0.906	−1.2

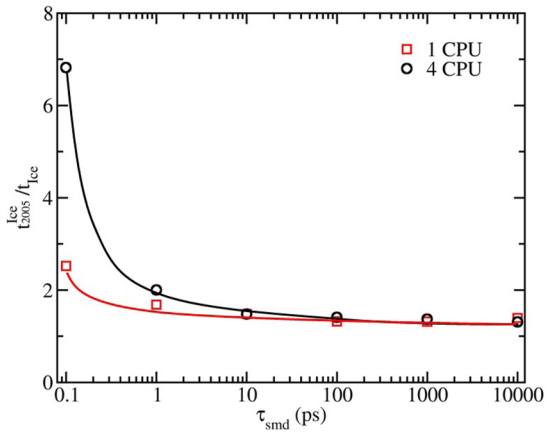

FIG. 8. Ratio between the clock time duration of simulations performed with the TIP4P$^{Ice}_{2005}$ and the TIP4P/Ice models, t^{Ice}_{2005}/t_{Ice}, as a function of τ_{smd}. Simulations span 10 ns of a liquid at 300 K and 1 bar containing 432 molecules. The study is performed using 4 and 1 CPU in the simulations as indicated in the legend.

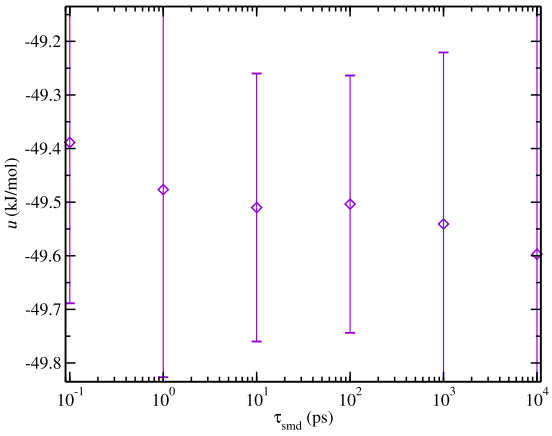

FIG. 9. Mean value of the potential energy (per mol) at 300 K for 50 ns runs as a function of τ_{smd}.

on relabeling would greatly exceed that invested in moving the molecules. On the other hand, too large τ_{smd}'s would result in the system evolving with wrongly labeled molecules and, therefore, in a simulation output that does not respond to the desired Hamiltonian. We first focus on the efficiency and then on the correctness of the simulations depending on the selected value for τ_{smd}.

To quantify the efficiency, we run 10 ns simulations of a liquid with the TIP4P$^{Ice}_{2005}$ and TIP4P/Ice models and measure the wall-clock time needed to complete each simulation. In Fig. 8, we show the ratio between the wall-clock times of these simulations, t^{Ice}_{2005}/t_{Ice}, as a function of τ_{smd}. The number of water molecules employed in these simulations is 432. A high ratio means low efficiency of the TMS simulation scheme, and vice versa. As can be seen, the ratio sharply increases for short τ_{smd}'s, whereas it asymptotically goes to a value slightly larger than 1 for large τ_{smd}'s. The reason why the ratio does not exactly reach 1 for large τ_{smd}'s is that, in the TMS model, there are two types of "molecules," and for the crossed interactions, all the distances between all sites of the interacting molecules are computed (16 distances for a TIP4P geometry). However, the GROMACS algorithm saves time for the interaction between molecules of the same species by considering only distances between interacting sites (10 in this case: the distances between the charges and that between the LJ sites). By comparing the red curve [1 central processing unit (CPU)] with the black curve (4 CPUs) in Fig. 8, it is clear that as the number of CPUs increases, the efficiency of using the TMS molecular model decreases for very small values of τ_{smd}. This is because parallelization reduces the time spent running the short molecular dynamics trajectories, and the time required to reassign identities becomes a more significant fraction of the total simulation time. For τ_{smd} = 10 ps, the value chosen in this work, the ratio is around 1.5, independent of the number of employed CPUs. Therefore, our TMS model that effectively incorporates polarizability can be implemented at a rather low computational cost.

We already know that a long τ_{smd} is preferable in terms of efficiency. However, as earlier discussed, long τ_{smd}'s may result in simulations that do not obey the proposed Hamiltonian. To assess the correctness of the simulations, we examine the dependence of several thermodynamic properties on τ_{smd}. We first have a look at the potential energy of a liquid at 300 K and 1 bar. In Fig. 9, we show that the potential energy does not appreciably depend on τ_{smd}. This result is somewhat expected because the potential energy of the TMS model can be obtained by linearly combining those of the single-state models via Eq. (1) [see Fig. 4(b)].

Analogously to the potential energy, the density or the enthalpy can also be obtained via a linear combination of the corresponding property of the single-state systems. One might then question the necessity of performing simulations of the TMS model at all. First of all, simulations are required to determine the molar fraction with which the single-state properties are combined to give rise to those of the TMS model. Moreover, when dealing with heterogeneous systems, such as those containing ice in contact with water, it is essential to perform simulations where the TMS model's Hamiltonian is imposed. Recall that all ice molecules belong to the TIP4P/Ice state due to their $\bar{q}_6$ distribution (see Fig. 2). Therefore, the identity of the molecules needs to be updated as ice grows or melts to obey the desired Hamiltonian.

Accordingly, the melting temperature obtained in direct coexistence simulations may depend on the frequency with which the molecular identities are reassigned. We test such dependency by evaluating the melting temperature with direct coexistence simulations using different τ_{smd}'s. The first configuration for such simulations contains a solid in contact with a liquid, where all molecules are properly labeled according to their $\bar{q}_6$. In Appendix A, we provide the time evolution of the potential energy for all the direct coexistence runs used to determine T_m as a function of τ_{smd}. We show such dependency in Fig. 10. As can be seen, there is a wide range of τ_{smd} for which the melting temperature is independent of the choice of τ_{smd}. The selected τ_{smd} value for this work, 10 ps, safely lies within such a range. It has been shown for the TIP4P/Ice model that ice growth takes at least 1 ns per Å.[73,113] Therefore, if the molecular identities are updated at shorter time scales, ice growth will proceed with the molecular identities dictated by our Hamiltonian, and the simulations will be correct. For large τ_{smd}'s, however,

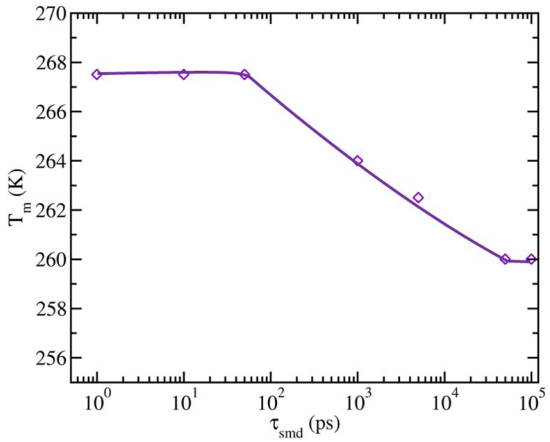

FIG. 10. Melting temperature computed via direct coexistence simulations using different τ_{smd} values. Symbols are actual calculations, and the line is a guide for the eye.

the obtained melting temperature goes down because the incorporation of molecules into the solid is not accompanied by a transition from the TIP4P/2005 to the TIP4P/Ice state. Therefore, the interactions that "glue" the solid molecules together are lower than required (recall that TIP4P/2005 has lower charges than TIP4P/Ice). As a consequence, the solid becomes less stable and the melting point goes down when increasing τ_{smd}, as shown in Fig. 9.

Therefore, in order to tune τ_{smd}, the time scale in which the structures identified with the selected order parameter transform into each other must be taken into account. In our case, we discriminate liquid-like from solid-like particles using $\tilde{q}_6$, and the relevant time scale for setting τ_{smd} is the time required for ice growth.

Had a different order parameter been used, then τ_{smd} would have had to be adapted to the relevant time scale for the evolution of the structures identified by that order parameter. In Sec. V, we show that the compressibility at low temperatures is enhanced by the TMS Hamiltonian (see Fig. 5), suggesting some degree of spatial correlation between molecular state and density domain. This correlation was captured with τ_{smd} = 10 ps, which suggests that this time is shorter than that required for density fluctuations. This statement is further supported by the fact that a simulation with τ_{smd} = 1 ps gives the same κ_T (indicated with a cross in Fig. 5 for T = 230 K).

In this work, we have opted to keep τ_{smd} fixed for any temperature. Alternatively, τ_{smd} could be made dependent on some physical timescale such as the structural relaxation time. This is an interesting idea that could be tested in the future. In any case, it is reassuring that there is a wide time window for which the results do not depend on the specific choice of τ_{smd} (see Figs. 5 and 10).

IX. COEXISTENCE VIA FREE ENERGY CALCULATIONS: A CONSISTENCY TEST

In this section, we test the consistency between the calculation of the melting temperature via direct coexistence (Fig. 6) and free energy calculations. In the latter approach, the free energy of each phase is separately obtained, and then the temperature of equal chemical potential determines T_m (at 1 bar pressure). For this test to be passed, the zero-point-energy difference between both states, ΔE^0 in Fig. 1, has to be properly computed. Therefore, this exercise serves as a double check for the correctness of our approach to obtain such energy difference.

The free energy of the solid, entirely composed of TIP4P/Ice molecules, was obtained at 250 and 270 K using the Einstein molecule version[87,88,91] of the Einstein crystal method.[114,115] The results of these calculations are indicated with blue triangles in Fig. 11. With the free energy at a single point (250 K) and integrating the enthalpy of the solid along temperature,[116] we get the chemical potential as a function of temperature (blue solid curve in Fig. 11). As a consistency test, we checked that the curve integrated from 250 K passes through the point calculated at 270 K.

To compute the free energy of the TIP4P$^{Ice}_{2005}$ liquid, we first calculate it for each of the single state models. For that purpose, we compute the free energy of the solid at the corresponding melting temperature (250 K for TIP4P/2005[110] and 270 K for TIP4P/Ice[111]) using the Einstein Molecule method. At such a state point, the free energies of the solid and of the liquid phases are equal to each other. Then, by integrating the enthalpy of the corresponding single-state liquid, we get the free energy of the TIP4P/2005 and TIP4P/Ice liquids along temperature. Then, we linearly combine the chemical potentials of the single-state liquids via Eq. (1). This approach is reasonable given that both the density and the enthalpy of the TMS model were successfully obtained with this approach (see Fig. 4). To improve our estimate of the TIP4P$^{Ice}_{2005}$ liquid chemical potential, we add the small enthalpy difference (about 0.05 kJ/mol) between the TMS model enthalpy and that of the ideal mix of the single-state models [see in Fig. 4(c)]. This gives the purple dashed chemical potential curve in Fig. 11. Apparently, the liquid chemical potential curve does not cross that of the solid, and a melting point cannot be found.

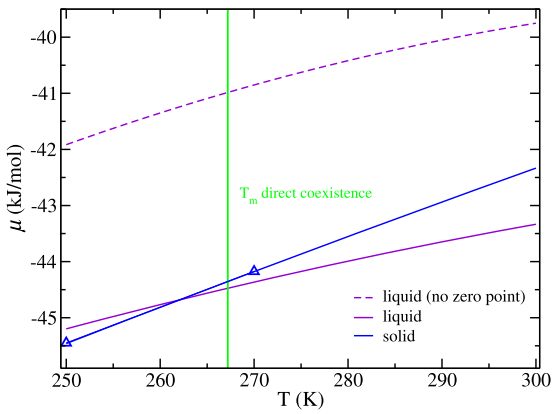

FIG. 11. Chemical potentials at 1 bar as a function of temperature for the TIP4P$^{Ice}_{2005}$ ice I_h (solid blue line) and liquid (solid purple line) phases (see main text for calculation details). All molecules in the solid are in the TIP4P/Ice state, whereas in the liquid, both states are present. The dashed purple line corresponds to the liquid chemical potential without correcting for the zero point energy of molecules in the TIP4P/2005 state (a $X_{TIP4P/2005}\Delta E^0_{Ice-2005}$ term has to be added to the dashed purple to get the solid purple line). The vertical green line corresponds to the melting temperature of TIP4P$^{Ice}_{2005}$ obtained via direct coexistence. The crossing between the solid blue and purple lines gives T_m through the chemical potential route.

The key is that we have not yet included the intra-molecular energy term in the liquid energy [second term in Eq. (4)]. Recall that the intra-molecular energy of the solid is 0, given that all molecules in the solid are in the TIP4P/Ice state and that we set $E^0_{TIP4P/Ice} = 0$. In the liquid, however, there is a mix of both states, and the energy should be corrected by $X_{TIP4P/2005}\Delta E^0_{Ice-2005}$. After adding such a term [which is temperature dependent because both $X_{TIP4P/2005}$ (Fig. 3) and $\Delta E^0_{Ice-2005}$ (Fig. 7) depend on temperature], we obtain the purple solid chemical potential curve for the TIP4P$^{Ice}_{2005}$ liquid. The dashed purple curve experiences a large shift to become the solid purple one, which now does cross the blue curve at $T_m = (264 \pm 5)$K. This result is consistent within the error bar with the melting temperature obtained via direct coexistence ($T_m = 267.5 \pm 2$). For our system size, the typical error from direct coexistence simulations is 2 K,[86] whereas we estimate a 5 K error for the chemical potential route, where the melting point is obtained through the crossing between two chemical potential lines that have a very similar slope (see blue and purple lines in Fig. 11). The melting temperature is then quite sensitive to errors in the determination of the chemical potentials of the liquid and the solid and by the uncertainty in the estimate of $\Delta E^0_{Ice-2005}$. The good consistency between the melting temperatures gives us great confidence in the approach followed to simulate the TMS model, particularly in the association we establish between ΔE^0 and the average inter-molecular energy change upon state transitions, $-\langle \Delta E^{inter}_{change} \rangle$ (see Sec. VII).

X. OVERVIEW OF MODEL PROPERTIES

In Table I, we report a few thermodynamic properties of the TIP4P$^{Ice}_{2005}$ model alongside those of the TIP4P/2005 and TIP4P/Ice models and the experimental values. To enable a visual comparison of the relative performance of the models, we show a bar graph in Fig. 12 with the percent deviation with respect to the experimental values of several thermodynamic properties. Overall, the TMS model has the best predicting ability.

We insist on the fact that in this work, we do not aim at proposing the definitive TMS model but rather to exemplify our strategy to model water as a combination of two (or several) interconvertible states to improve the predictive ability of the simulations at a relatively low computational cost.

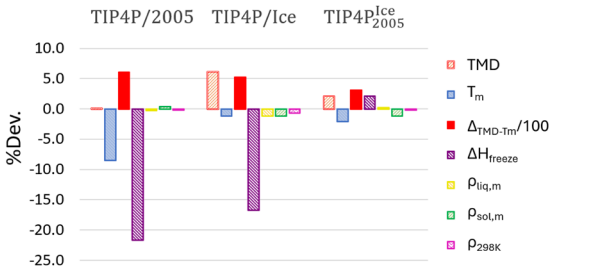

FIG. 12. Percent deviation of the model prediction with respect to the experimental value for several thermodynamic properties of interest. The performances of the TIP4P/2005, TIP4P/Ice, and TIP4P$^{Ice}_{2005}$ models are compared as indicated in the figure. The bar corresponding to the TMD-T_m difference (in red) has been divided by 100 in order to keep it visually comparable to the other bars. The subscripts *liq,m sol,m* stand for the liquid and solid at the melting temperature, respectively.

In any case, it is perhaps fair to acknowledge that the proposed model, TIP4P$^{Ice}_{2005}$, is quite competitive because it improves two already successful and widely used models, TIP4P/2005 and TIP4P/Ice, at a relatively cheap computational cost (1.5 slowdown factor). In particular, it greatly improves the prediction of the melting enthalpy made by the single-state models, which underestimate ΔH_m by about 15%–20%. In contrast, the new TSM model only overestimates it by 2% (see purple bars in Fig. 12). Finally, it is also worth mentioning that the TMS model is able to reduce the difference between the melting temperature and the TMD by almost 10° with respect to the best prediction of the single state models. This is not trivial, since most water models struggle to provide the experimental difference of 4 K (most rigid non-polarizable models estimate a difference of at least 25 K).[44,117]

XI. SUMMARY AND DISCUSSION

In summary, we propose a simulation approach in which molecules can acquire different states depending on their local molecular environment. Each state is a different non-polarizable model. We apply this idea to water by assigning the TIP4P/2005 and TIP4P/Ice rigid models to molecules with high- and low-tetrahedral environments, respectively. In this way, tetrahedrally coordinated molecules interact more favorably with each other than those in loosely ordered environments. This scheme effectively introduces polarization effects in the simulation at a relatively low cost from a computational point of view (simulations with the two-molecular-states water model are only about 1.5 times slower than standard single-state simulations).

Transitions from one state to another are made effective according to a threshold in the order parameter used to identify local order ($\tilde{q}_6$[45] in the present work). After running a short (10 ps) molecular dynamics window, particles are invariably assigned a state according to their respective $\tilde{q}_6$ value. In our proposed Hamiltonian, the intra-molecular potential energy change associated with the transition from one state to another is equal, but with the opposite sign, to the average inter-molecular potential energy change. To test the validity of this idea, we showed the consistency between the melting temperature obtained from direct coexistence simulations (of ice I_h in contact with liquid water) and that found from free energy calculations of the bulk phases separately.

For the sake of computational efficiency, transitions between states are not performed every molecular dynamics step. We test the impact of this approximation on the simulation output and conclude that it is enough to update molecular identities in a time scale faster than that required for ice growth. This timescale is associated with the fact that the selected order parameter discriminates ice-like from liquid-like environments. If an order parameter that is sensitive to another structural feature was employed, then a different time scale for updating the molecular states could be needed.

The two-state model we present in this work, which we call TIP4P$^{Ice}_{2005}$, performs overall better than either of the rigid models that build it. In particular, it significantly improves the prediction of the melting enthalpy, which is largely underestimated by TIP4P/2005 or TIP4P/Ice. The isothermal compressibility of TIP4P$^{Ice}_{2005}$ is also closer to the experiment as it is enhanced due to a

correlation between density and state population (such correlation is in line with the density-order parameter correlations shown in Ref. 102). The compressibility enhancement, however, is not sufficiently large to bring simulation predictions close to the experiment. In the future, it would be interesting to explore if compressibility can be further enhanced by using our approach in combination with order parameters specifically devised to identify molecules belonging to high and low-liquid density regions.[54,96,98,99,101–103,118–122] In any case, with this work we do not aim at proposing the best possible model within this simulation strategy but rather at demonstrating the feasibility and the applicability of the strategy itself, which can pave the way for the development of a highly competitive water model in terms of efficiency and predictive ability.

There are in the literature several simulation approaches that resemble what we do in this work. One is a minimal lattice three-state model developed to understand water polyamorphism.[123,124] The states in this model, which is inspired by the view that water is a mix of two liquids of different density,[30,49–56,125] represent molecular *superstructures*, and the transitions between them are regulated by their energy and entropy difference (so they are in chemical equilibrium with each other). In contrast, the states in our approach correspond to single molecules, and the transitions between them are dictated by the local molecular environment, in closer resemblance to standard polarizable models.[39,126–132] Our simulation scheme also reminds us of the embedded atom method employed to simulate metallic systems, where pairwise interactions are complemented with an embedding term obtained through the electron density created on each atomic location by the remainder of the atoms.[133] This extra term, however, cannot be viewed as a state acquired by the atom but rather as an effective many-atom interaction that does not affect pairwise interactions. Finally, in Ref. 134, an approach similar to ours was employed to enhance the rigidification of protein condensates by dynamically increasing the interactions between aromatic-rich domains following a criterion based on local structure (local density in this particular case). These simulations, though, led to out-of-equilibrium structures, and the implications of a two-state modeling on thermodynamic equilibrium were not assessed.

The scheme we propose is not necessarily restricted to representing water with two states. Multiple states could be incorporated into the model. Our strategy can improve the modeling of electrolyte aqueous solutions by assigning different states to bulk and to solvation water or by dynamically changing the interaction parameters of ions depending on their local environment (for instance, depending on whether they are solvated by water or forming an ionic solid).

ACKNOWLEDGMENTS

This project has been funded by Grant Nos. PID2019-105898GB-C21 and PID2022-136919NB-C31 of the Spanish Ministry of Science and Innovation. E.G.N. acknowledges Agencia Estatal de Investigación and Fondo Europeo de Desarrollo Regional

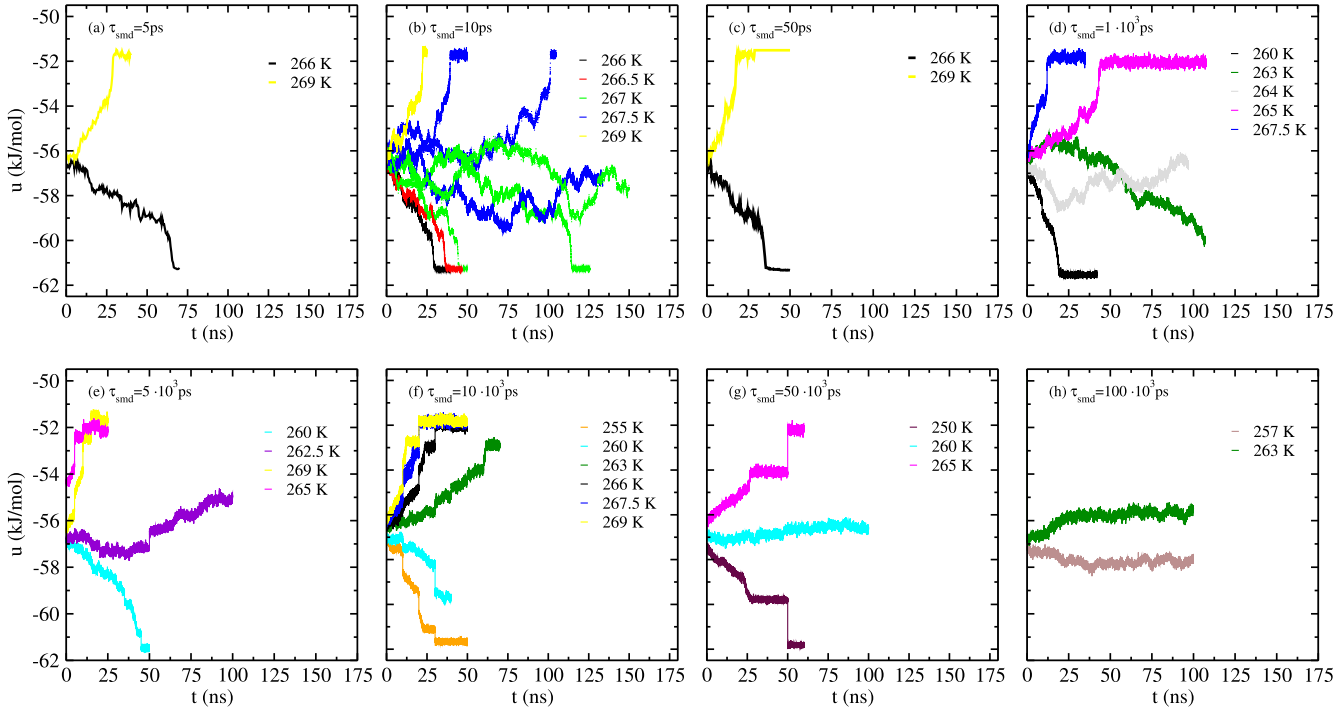

FIG. 13. Potential energy (per mol) vs time along direct coexistence runs. Each plot shows trajectories at different temperatures (see legend) and corresponds to a different value of τ_{smd} (as indicated inside the plot).

(FEDER), Grant Nos. PID2020-115722GB-C21 and PID2023-151751NB-100. L.F.S. acknowledges Ministerio de Universidades for a predoctoral Formación Profesorado Universitario Grant No. FPU22/02900.

AUTHOR DECLARATIONS

Conflict of Interest

The authors have no conflicts to disclose.

Author Contributions

Lucía F. Sedano: Conceptualization (equal); Data curation (equal); Formal analysis (equal); Investigation (equal); Methodology (equal); Resources (equal); Software (equal); Validation (equal); Visualization (equal); Writing – original draft (equal); Writing – review & editing (equal). **Carlos Vega**: Conceptualization (equal); Data curation (equal); Formal analysis (equal); Funding acquisition (equal); Investigation (equal); Methodology (equal); Project administration (equal); Resources (equal); Supervision (equal); Validation (equal); Writing – original draft (equal); Writing – review & editing (equal). **Eva G. Noya**: Data curation (equal); Formal analysis (equal); Funding acquisition (equal); Investigation (equal); Methodology (equal); Project administration (equal); Resources (equal); Software (equal); Supervision (equal); Validation (equal); Writing – review & editing (equal). **Eduardo Sanz**: Conceptualization (equal); Data curation (equal); Formal analysis (equal); Funding acquisition (equal); Investigation (equal); Methodology (equal); Project administration (equal); Supervision (equal); Validation (equal); Writing – original draft (equal); Writing – review & editing (equal).

DATA AVAILABILITY

The data that support the findings of this study are available within the article.

APPENDIX A: OBTAINING T_m AS A FUNCTION OF τ_{smd}

We provide here the direct coexistence runs used to build Fig. 10. In Fig. 13, we show, for each studied value of τ_{smd}, the potential energy during direct coexistence simulations starting from a configuration of ice in contact with liquid water (see Sec. IV for further details). In the initial configuration, each molecule is properly assigned either the TIP4P/Ice or the TIP4P/2005 state depending on its $\bar{q}_6$ value. The molecular states are not updated until the beginning of the following molecular dynamics window.

Interestingly, in some cases (see, e.g., the plot corresponding to $\tau_{smd} = 10 \times 10^3$ ps in Fig. 13), abrupt steps in the potential energy can be appreciated. These steps coincide with the moment in which a new molecular dynamics window is started. This is due to the fact that, along a given window, there are molecules that cross the $\bar{q}_6$ threshold (either by incorporating into ice from the liquid or vice versa) without changing state accordingly. Such a state change is made effective when a new trajectory is restarted, which causes a sudden jump in the potential energy. These jumps are not appreciated when τ_{smd} is short, given that molecules are reassigned state as they incorporate into either phase.

APPENDIX B: TUNING $\bar{q}_{6t}$

We chose $\bar{q}_{6,t} = 0.25$ because, as shown in this appendix, the prediction of thermodynamic properties by the TMS model worsens by either increasing or decreasing such a threshold. The targeted properties are summarized in Fig. 15. In Fig. 14(a), we show the difference between the model and the experimental values for the following temperatures: T_m (blue), TMD (green), and TMD-T_m (red) as a function of $\bar{q}_{6,t}$. Recall that $\bar{q}_{6,t} = 0.25$ corresponds to the TIP4P$^{Ice}_{2005}$ model presented in this work, whereas the other $\bar{q}_{6,t}$ values correspond to alternative models where the transition between the TIP4P/2005 and TIP4P/Ice states is dictated by another threshold. The best melting temperature is predicted by the model with $\bar{q}_{6,t} = 0.2$. However, this model gives the worst TMD. Overall, $\bar{q}_{6,t} = 0.25$ provides the best balance in predicting T_m, the TMD, and their difference. In Fig. 14(b), we show the melting enthalpy as a function of $\bar{q}_{6t}$. As can be seen, the best prediction corresponds to $\bar{q}_{6,t} = 0.25$, i.e., to the TIP4P$^{Ice}_{2005}$ model. In Fig. 15, we present, with a bar graph analogous to that presented in Fig. 12, the relative deviation between the model prediction and the experimental value for several thermodynamic properties and for the three $\bar{q}_{6,t}$ values

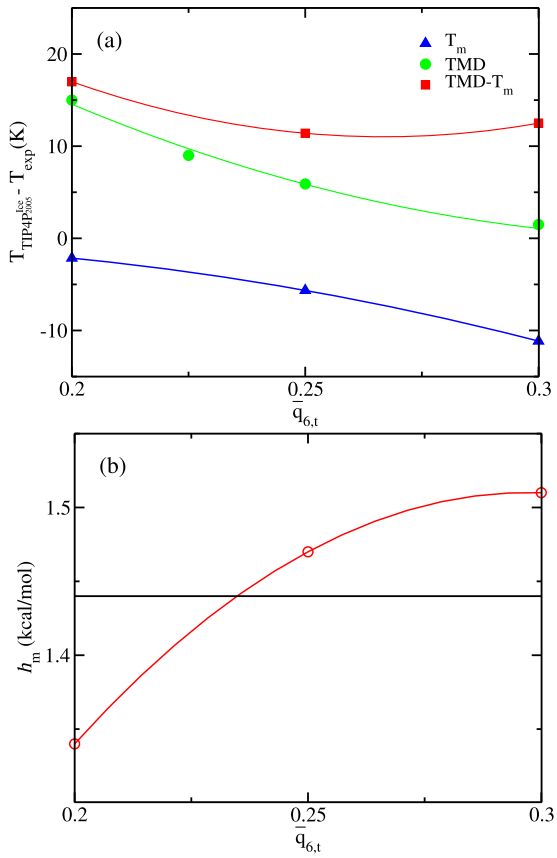

FIG. 14. (a) Difference between the model and the experimental values for the following temperatures: T_m (blue), TMD (green), and TMD-T_m (red) as a function of $\bar{q}_{6,t}$. (b) Molar melting enthalpy as a function of $\bar{q}_{6,t}$. The solid black line represents the experimental value.

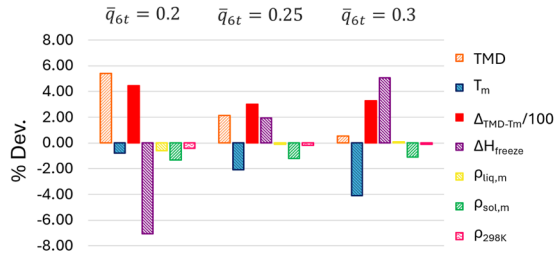

FIG. 15. Percent deviation of the TIP4P$^{Ice}_{2005}$ prediction with respect to the experiment for different $\bar{q}_{6,t}$ values and for several thermodynamic properties of interest. The performances of three TMS models with different $\bar{q}_{6,t}$ thresholds for switching between TIP4P/2005 and TIP4P/Ice are compared (the TIP4P$^{Ice}_{2005}$ model corresponds to $\bar{q}_{6,t} = 0.25$). The bar corresponding to the TMD-T_m difference (in red) has been divided by 100 in order to keep it visually comparable to the other bars. The subscripts *liq,m sol,m* stand for the liquid and the solid at the melting temperature, respectively.

compared in this section. Clearly, $\bar{q}_{6,t} = 0.25$ gives the best overall performance.

REFERENCES

[1] T. Nakamuro, M. Sakakibara, H. Nada, K. Harano, and E. Nakamura, "Capturing the moment of emergence of crystal nucleus from disorder," J. Am. Chem. Soc. **143**(4), 1763–1767 (2021).

[2] K. H. Kim, K. Amann-Winkel, N. Giovambattista, A. Späh, F. Perakis, H. Pathak, M. L. Parada, C. Yang, D. Mariedahl, T. Eklund *et al.*, "Experimental observation of the liquid-liquid transition in bulk supercooled water under pressure," Science **370**(6519), 978–982 (2020).

[3] P. G. Debenedetti, F. Sciortino, and G. H. Zerze, "Second critical point in two realistic models of water," Science **369**(6501), 289–292 (2020).

[4] P. M. Piaggi, J. Weis, A. Z. Panagiotopoulos, P. G. Debenedetti, and R. Car, "Homogeneous ice nucleation in an ab initio machine-learning model of water," Proc. Natl. Acad. Sci. U. S. A. **119**(33), e2207294119 (2022).

[5] W. L. Jorgensen, J. Chandrasekhar, J. D. Madura, R. W. Impey, and M. L. Klein, "Comparison of simple potential functions for simulating liquid water," J. Chem. Phys. **79**(2), 926–935 (1983).

[6] H. J. C. Berendsen, J. R. Grigera, and T. P. Straatsma, "The missing term in effective pair potentials," J. Phys. Chem. **91**(24), 6269–6271 (1987).

[7] J. D. Bernal, R. H. Fowler *et al.*, "A theory of water and ionic solution, with particular reference to hydrogen and hydroxyl ions," J. Chem. Phys. **1**(8), 515–548 (1933).

[8] H. W. Horn, W. C. Swope, J. W. Pitera, J. D. Madura, T. J. Dick, G. L. Hura, and T. Head-Gordon, "Development of an improved four-site water model for biomolecular simulations: TIP4P-Ew," J. Chem. Phys. **120**(20), 9665–9678 (2004).

[9] J. L. F. Abascal and C. Vega, "A general purpose model for the condensed phases of water: TIP4P/2005," J. Chem. Phys. **123**(23), 234505 (2005).

[10] J. Abascal, E. Sanz, R. García Fernández, and C. Vega, "A potential model for the study of ices and amorphous water: TIP4P/Ice," J. Chem. Phys. **122**(23), 234511 (2005).

[11] S. Izadi, R. Anandakrishnan, and A. V. Onufriev, "Building water models: A different approach," J. Phys. Chem. Lett. **5**, 3863–3871 (2014).

[12] V. Molinero and E. B. Moore, "Water modeled as an intermediate element between carbon and silicon," J. Phys. Chem. B **113**(13), 4008–4016 (2009).

[13] C. Vega and J. L. F. Abascal, "Simulating water with rigid non-polarizable models: A general perspective," Phys. Chem. Chem. Phys. **13**(44), 19663–19688 (2011).

[14] L. F. Sedano, S. Blazquez, and C. Vega, "Accuracy limit of non-polarizable four-point water models: TIP4P/2005 vs OPC. Should water models reproduce the experimental dielectric constant?," J. Chem. Phys. **161**(4), 044505 (2024).

[15] S. A. Clough, Y. Beers, G. P. Klein, and L. S. Rothman, "Dipole moment of water from Stark measurements of H_2O, HDO, and D_2O," J. Chem. Phys. **59**(5), 2254–2259 (1973).

[16] P. L. Silvestrelli and M. Parrinello, "Water molecule dipole in the gas and in the liquid phase," Phys. Rev. Lett. **82**(16), 3308 (1999).

[17] M. A. González and J. L. Abascal, "A flexible model for water based on TIP4P/2005," J. Chem. Phys. **135**(22), 224516 (2011).

[18] S. Habershon, T. E. Markland, and D. E. Manolopoulos, "Competing quantum effects in the dynamics of a flexible water model," J. Chem. Phys. **131**(2), 024501 (2009).

[19] Y. Wu, H. L. Tepper, and G. A. Voth, "Flexible simple point-charge water model with improved liquid-state properties," J. Chem. Phys. **124**(2), 024503 (2006).

[20] K. Laasonen, M. Sprik, M. Parrinello, and R. Car, "'*Ab initio*' liquid water," J. Chem. Phys. **99**(11), 9080–9089 (1993).

[21] R. Car and M. Parrinello, "Unified approach for molecular dynamics and density-functional theory," Phys. Rev. Lett. **55**(22), 2471 (1985).

[22] R. A. Friesner, "*Ab initio* quantum chemistry: Methodology and applications," Proc. Natl. Acad. Sci. U. S. A. **102**(19), 6648–6653 (2005).

[23] M. J. Gillan, D. Alfe, and A. Michaelides, "Perspective: How good is DFT for water?," J. Chem. Phys. **144**(13), 130901 (2016).

[24] J. Behler, "Neural network potential-energy surfaces in chemistry: A tool for large-scale simulations," Phys. Chem. Chem. Phys. **13**(40), 17930–17955 (2011).

[25] L. Zhang, J. Han, H. Wang, R. Car, and E. Weinan, "Deep potential molecular dynamics: A scalable model with the accuracy of quantum mechanics," Phys. Rev. Lett. **120**(14), 143001 (2018).

[26] Y. Zhang, H. Wang, W. Chen, J. Zeng, L. Zhang, H. Wang, and E. Weinan, "DP-GEN: A concurrent learning platform for the generation of reliable deep learning based potential energy models," Comput. Phys. Commun. **253**, 107206 (2020).

[27] L. Zhang, H. Wang, R. Car, and W. E, "Phase diagram of a deep potential water model," Phys. Rev. Lett. **126**(23), 236001 (2021).

[28] O. Wohlfahrt, C. Dellago, and M. Sega, "*Ab initio* structure and thermodynamics of the RPBE-D3 water/vapor interface by neural-network molecular dynamics," J. Chem. Phys. **153**(14), 144710 (2020).

[29] P. Montero de Hijes, S. Romano, A. Gorfer, and C. Dellago, "The kinetics of the ice–water interface from *ab initio* machine learning simulations," J. Chem. Phys. **158**(20), 204706 (2023).

[30] T. E. Gartner III, L. Zhang, P. M. Piaggi, R. Car, A. Z. Panagiotopoulos, and P. G. Debenedetti, "Signatures of a liquid–liquid transition in an ab initio deep neural network model for water," Proc. Natl. Acad. Sci. U. S. A. **117**(42), 26040–26046 (2020).

[31] P. M. de Hijes, C. Dellago, R. Jinnouchi, and G. Kresse, "Density isobar of water and melting temperature of ice: Assessing common density functionals," J. Chem. Phys. **161**, 131102 (2024).

[32] G. Lamoureux, A. D. MacKerell, and B. Roux, "A simple polarizable model of water based on classical Drude oscillators," J. Chem. Phys. **119**(10), 5185–5197 (2003).

[33] J. A. Lemkul, J. Huang, B. Roux, and A. D. MacKerell, Jr., "An empirical polarizable force field based on the classical Drude oscillator model: Development history and recent applications," Chem. Rev. **116**, 4983 (2016).

[34] P. Paricaud, M. Předota, A. A. Chialvo, and P. T. Cummings, "From dimer to condensed phases at extreme conditions: Accurate predictions of the properties of water by a Gaussian charge polarizable model," J. Chem. Phys. **122**, 244511 (2005).

[35] P. Ren and J. W. Ponder, "Polarizable atomic multipole water model for molecular mechanics simulation," J. Phys. Chem. B **107**, 5933 (2003).

[36] L.-P. Wang, T. Head-Gordon, J. W. Ponder, P. Ren, J. D. Chodera, P. K. Eastman, T. J. Martinez, and V. S. Pande, "Systematic improvement of a classical molecular model of water," J. Phys. Chem. B **117**, 9956–9972 (2013).

[37] P. T. Kiss and A. Baranyai, "A systematic development of a polarizable potential of water," J. Chem. Phys. **138**, 204507 (2013).

[38] H. Jiang, O. A. Moultos, I. G. Economou, and A. Z. Panagiotopoulos, "Hydrogen-bonding polarizable intermolecular potential model for water," J. Phys. Chem. B **120**, 12358–12370 (2016).

[39] S. W. Rick, S. J. Stuart, and B. J. Berne, "Dynamical fluctuating charge force fields: Application to liquid water," J. Chem. Phys. **101**(7), 6141–6156 (1994).

[40]V. Babin, C. Leforestier, and F. Paesani, "Development of a 'first principles' water potential with flexible monomers: Dimer potential energy surface, VRT spectrum, and second virial coefficient," J. Chem. Theory Comput. **9**, 5395 (2013).
[41]G. A. Cisneros, K. T. Wikfeldt, L. Ojamae, J. Lu, Y. Xu, H. Torabifard, A. P. Bartok, G. Csanyi, V. Molinero, and F. Paesani, "Modeling molecular interactions in water: From pairwise to many-body potential energy functions," Chem. Rev. **116**, 7501 (2016).
[42]Q. Yu, C. Qu, P. L. Houston, R. Conte, A. Nandi, and J. M. Bowman, "q-AQUA: A many-body CCSD(T) water potential, including four-body interactions, demonstrates the quantum nature of water from clusters to the liquid phase," J. Phys. Chem. Lett. **13**, 5068 (2022).
[43]G. S. Fanourgakis and S. S. Xantheas, "Development of transferable interaction potentials for water. V. Extension of the flexible, polarizable, Thole-type model potential (TTM3-F, v. 3.0) to describe the vibrational spectra of water clusters and liquid water," J. Chem. Phys. **128**, 074506 (2008).
[44]S. Blazquez and C. Vega, "Melting points of water models: Current situation," J. Chem. Phys. **156**, 216101 (2022).
[45]W. Lechner and C. Dellago, "Accurate determination of crystal structures based on averaged local bond order parameters," J. Chem. Phys. **129**(11), 114707 (2008).
[46]I. Skarmoutsos, G. Franzese, and E. Guardia, "Using Car-Parrinello simulations and microscopic order descriptors to reveal two locally favored structures with distinct molecular dipole moments and dynamics in ambient liquid water," J. Mol. Liq. **364**, 119936 (2022).
[47]I. Skarmoutsos, M. Masia, and E. Guardia, "Structural and dipolar fluctuations in liquid water: A Car–Parrinello molecular dynamics study," Chem. Phys. Lett. **648**, 102 (2016).
[48]E. Guardia, I. Skarmoutsos, and M. Masia, "Hydrogen bonding and related properties in liquid water: A Car–Parrinello molecular dynamics simulation study," J. Phys. Chem. B **119**, 8926 (2015).
[49]N. Novak, X. Liang, and G. M. Kontogeorgis, "Prediction of water anomalous properties by introducing the two-state theory in SAFT," J. Chem. Phys. **160**(10), 104505 (2024).
[50]P. H. Poole, F. Sciortino, T. Grande, H. E. Stanley, and C. A. Angell, "Effect of hydrogen bonds on the thermodynamic behavior of liquid water," Phys. Rev. Lett. **73**, 1632–1635 (1994).
[51]M. Simões, A. Steudel, and A. P. R. Santos, "Liquid water: A single approach to its two continuous phase transitions," J. Phys. Chem. B **127**(4), 955–960 (2023).
[52]V. Holten and M. A. Anisimov, "Entropy-driven liquid–liquid separation in supercooled water," Sci. Rep. **2**(1), 713 (2012).
[53]V. Holten, J. C. Palmer, P. H. Poole, P. G. Debenedetti, and M. A. Anisimov, "Two-state thermodynamics of the ST2 model for supercooled water," J. Chem. Phys. **140**(10), 104502 (2014).
[54]J. Russo and H. Tanaka, "Understanding water's anomalies with locally favoured structures," Nat. Commun. **5**(1), 3556 (2014).
[55]R. S. Singh, J. W. Biddle, P. G. Debenedetti, and M. A. Anisimov, "Two-state thermodynamics and the possibility of a liquid-liquid phase transition in supercooled TIP4P/2005 water," J. Chem. Phys. **144**(14), 144504 (2016).
[56]P. Gallo, K. Amann-Winkel, C. A. Angell, M. A. Anisimov, F. Caupin, C. Chakravarty, E. Lascaris, T. Loerting, A. Z. Panagiotopoulos, J. Russo *et al.*, "Water: A tale of two liquids," Chem. Rev. **116**(13), 7463–7500 (2016).
[57]I. Nezbeda, F. Moučka, and W. R. Smith, "Recent progress in molecular simulation of aqueous electrolytes: Force fields, chemical potentials and solubility," Mol. Phys. **114**(11), 1665–1690 (2016).
[58]I. S. Joung and T. E. Cheatham III, "Determination of alkali and halide monovalent ion parameters for use in explicitly solvated biomolecular simulations," J. Phys. Chem. B **112**(30), 9020–9041 (2008).
[59]D. E. Smith and L. X. Dang, "Computer simulations of NaCl association in polarizable water," J. Chem. Phys. **100**(5), 3757–3766 (1994).
[60]Z. R. Kann and J. L. Skinner, "A scaled-ionic-charge simulation model that reproduces enhanced and suppressed water diffusion in aqueous salt solutions," J. Chem. Phys. **141**(10), 104507 (2014).
[61]T. Martinek, E. Duboué-Dijon, Š. Timr, P. E. Mason, K. Baxová, H. E. Fischer, B. Schmidt, E. Pluhařová, and P. Jungwirth, "Calcium ions in aqueous solutions: Accurate force field description aided by ab initio molecular dynamics and neutron scattering," J. Chem. Phys. **148**(22), 222813 (2018).
[62]M. Kohagen, P. E. Mason, and P. Jungwirth, "Accounting for electronic polarization effects in aqueous sodium chloride via molecular dynamics aided by neutron scattering," J. Phys. Chem. B **120**(8), 1454–1460 (2016).
[63]V. M. Trejos, M. de Lucas, C. Vega, S. Blazquez, and F. Gámez, "Further extension of the Madrid-2019 force field: Parametrization of nitrate (NO_3^-) and ammonium (NH_4^+) ions," J. Chem. Phys. **159**(22), 224501 (2023).
[64]S. Blazquez, I. C. Bourg, and C. Vega, "Madrid-2019 force field: An extension to divalent cations Sr^{2+} and Ba^{2+}," J. Chem. Phys. **160**(4), 046101 (2024).
[65]E. Duboué-Dijon, P. E. Mason, H. E. Fischer, and P. Jungwirth, "Hydration and ion pairing in aqueous Mg^{2+} and Zn^{2+} solutions: Force-field description aided by neutron scattering experiments and ab initio molecular dynamics simulations," J. Phys. Chem. B **122**(13), 3296–3306 (2017).
[66]R. Fuentes-Azcatl and M. C. Barbosa, "Sodium chloride, NaCl/ϵ: New force field," J. Phys. Chem. B **120**(9), 2460–2470 (2016).
[67]H. Jiang, Z. Mester, O. A. Moultos, I. G. Economou, and A. Z. Panagiotopoulos, "Thermodynamic and transport properties of H_2O + NaCl from polarizable force fields," J. Chem. Theory Comput. **11**(8), 3802–3810 (2015).
[68]F. Moucka, I. Nezbeda, and W. R. Smith, "Chemical potentials, activity coefficients, and solubility in aqueous NaCl solutions: Prediction by polarizable force fields," J. Chem. Theory Comput. **11**(4), 1756–1764 (2015).
[69]A. Caruso, X. Zhu, J. L. Fulton, and F. Paesani, "Accurate modeling of bromide and iodide hydration with data-driven many-body potentials," J. Phys. Chem. B **126**(41), 8266–8278 (2022).
[70]F. Paesani, P. Bajaj, and M. Riera, "Chemical accuracy in modeling halide ion hydration from many-body representations," Adv. Phys.: X **4**(1), 1631212 (2019).
[71]J. R. Espinosa, C. Vega, and E. Sanz, "Homogeneous ice nucleation rate in water droplets," J. Phys. Chem. C **122**(40), 22892–22896 (2018).
[72]J. R. Espinosa, C. Vega, C. Valeriani, and E. Sanz, "Seeding approach to crystal nucleation," J. Chem. Phys. **144**(3), 034501 (2016).
[73]J. R. Espinosa, C. Navarro, E. Sanz, C. Valeriani, and C. Vega, "On the time required to freeze water," J. Chem. Phys. **145**(21), 211922 (2016).
[74]E. Sanz, C. Vega, J. Abascal, and L. MacDowell, "Phase diagram of water from computer simulation," Phys. Rev. Lett. **92**(25), 255701 (2004).
[75]E. Sanz, C. Vega, J. Espinosa, R. Caballero-Bernal, J. Abascal, and C. Valeriani, "Homogeneous ice nucleation at moderate supercooling from molecular simulation," J. Am. Chem. Soc. **135**(40), 15008–15017 (2013).
[76]B. Hess, C. Kutzner, D. van der Spoel, and E. Lindahl, "GROMACS 4: Algorithms for highly efficient, load-balanced, and scalable molecular simulation," J. Chem. Theory Comput. **4**, 435–447 (2008).
[77]M. Parrinello and A. Rahman, "Polymorphic transitions in single crystals: A new molecular dynamics method," J. Appl. Phys. **52**(12), 7182–7190 (1981).
[78]S. Nosé, "A molecular dynamics method for simulations in the canonical ensemble," Mol. Phys. **52**, 255–268 (1984).
[79]W. G. Hoover, "Canonical dynamics: Equilibrium phase-space distributions," Phys. Rev. A **31**, 1695–1697 (1985).
[80]M. P. Allen and D. J. Tildesley, *Computer Simulations of Liquids* (Oxford Science Publications, Oxford, 1987).
[81]A. J. C. Ladd and L. V. Woodcock, Chem. Phys. Lett. **51**, 155 (1977).
[82]A. J. C. Ladd and L. V. Woodcock, Mol. Phys. **36**, 611 (1978).
[83]T. Darden, D. York, and L. Pedersen, "Particle mesh Ewald: An $N\log(N)$ method for Ewald sums in large systems," J. Chem. Phys. **98**, 10089–10092 (1993).
[84]U. Essmann, L. Perera, M. L. Berkowitz, T. Darden, H. Lee, and L. G. Pedersen, "A smooth particle mesh Ewald method," J. Chem. Phys. **103**, 8577–8593 (1995).
[85]B. Hess, H. Bekker, H. J. C. Berendsen, and J. G. E. M. Fraaije, "LINCS: A linear constraint solver for molecular simulations," J. Comput. Chem. **18**, 1463–1472 (1997).
[86]M. M. Conde, M. Rovere, and P. Gallo, "High precision determination of the melting points of water TIP4P/2005 and water TIP4P/Ice models by the direct coexistence technique," J. Chem. Phys. **147**(24), 244506 (2017).
[87]C. Vega and E. G. Noya, "Revisiting the Frenkel-Ladd method to compute the free energy of solids: The Einstein molecule approach," J. Chem. Phys. **127**(15), 154113 (2007).
[88]E. G. Noya, M. M. Conde, and C. Vega, "Computing the free energy of molecular solids by the Einstein molecule approach: Ices XIII and XIV, hard-dumbbells and a patchy model of proteins," J. Chem. Phys. **129**, 104704 (2008).

[89]V. Buch, P. Sandler, and J. Sadlej, "Simulations of H_2O solid, liquid, and clusters, with an emphasis on ferroelectric ordering transition in hexagonal ice," J. Phys. Chem. B **102**, 8641 (1998).
[90]P. N. Swarztrauber, "On computing the points and weights for Gauss–Legendre quadrature," SIAM J. Sci. Comput. **24**(3), 945–954 (2003).
[91]J. L. Aragones, E. G. Noya, C. Valeriani, and C. Vega, "Free energy calculations for molecular solids using GROMACS," J. Chem. Phys. **139**, 034104 (2013).
[92]P. Wernet, D. Nordlund, U. Bergmann, M. Cavalleri, M. Odelius, H. Ogasawara, L. A. Näslund, T. Hirsch, L. Ojamäe, P. Glatzel *et al.*, "The structure of the first coordination shell in liquid water," Science **304**(5673), 995–999 (2004).
[93]C. Huang, K. T. Wikfeldt, T. Tokushima, D. Nordlund, Y. Harada, U. Bergmann, M. Niebuhr, T. Weiss, Y. Horikawa, M. Leetmaa *et al.*, "The inhomogeneous structure of water at ambient conditions," Proc. Natl. Acad. Sci. U. S. A. **106**(36), 15214–15218 (2009).
[94]R. J. Speedy and C. A. Angell, "Isothermal compressibility of supercooled water and evidence for a thermodynamic singularity at −45 °C," J. Chem. Phys. **65**(3), 851–858 (1976).
[95]S. Sastry, P. G. Debenedetti, F. Sciortino, and H. E. Stanley, "Singularity-free interpretation of the thermodynamics of supercooled water," Phys. Rev. E **53**, 6144–6154 (1996).
[96]K. T. Wikfeldt, A. Nilsson, and L. G. M. Pettersson, "Spatially inhomogeneous bimodal inherent structure of simulated liquid water," Phys. Chem. Chem. Phys. **13**(44), 19918–19924 (2011).
[97]L. Landau and E. M. Lifschitz, *Statistical Physics* (Addison-Wesley; Pergamon Press, London; Reading, MA, 1958).
[98]E. Shiratani and M. Sasai, "Molecular scale precursor of the liquid–liquid phase transition of water," J. Chem. Phys. **108**(8), 3264–3276 (1998).
[99]J. R. Errington and P. G. Debenedetti, "Relationship between structural order and the anomalies of liquid water," Nature **409**, 318–321 (2001).
[100]J. M. Montes de Oca, F. Sciortino, and G. A. A. Appignanesi, "A structural indicator for water built upon potential energy considerations," J. Chem. Phys. **152**, 244503 (2020).
[101]A. V. Muthachikavil, G. M. Kontogeorgis, X. Liang, Q. Lei, and B. Peng, "Structural characteristics of low-density environments in liquid water," Phys. Rev. E **105**, 034604 (2022).
[102]R. Foffi and F. Sciortino, "Correlated fluctuations of structural indicators close to the liquid–liquid transition in supercooled water," J. Phys. Chem. B **127**(1), 378–386 (2023).
[103]A. Neophytou, D. Chakrabarti, and F. Sciortino, "Topological nature of the liquid–liquid phase transition in tetrahedral liquids," Nat. Phys. **18**(10), 1248–1253 (2022).
[104]H. L. Pi, J. L. Aragones, C. Vega, E. G. Noya, J. L. Abascal, M. A. Gonzalez, and C. McBride, "Anomalies in water as obtained from computer simulations of the TIP4P/2005 model: Density maxima, and density, isothermal compressibility and heat capacity minima," Mol. Phys. **107**(4–6), 365–374 (2009).
[105]J. R. Espinosa, J. L. F. Abascal, L. F. Sedano, E. Sanz, and C. Vega, "On the possible locus of the liquid–liquid critical point in real water from studies of supercooled water using the TIP4P/Ice model," J. Chem. Phys. **158**(20), 204505 (2023).
[106]V. Holten, J. V. Sengers, and M. A. Anisimov, "Equation of state for supercooled water at pressures up to 400 MPa," J. Phys. Chem. Ref. Data **43**, 043101 (2014).
[107]D. E. Hare and C. M. Sorensen, "The density of supercooled water. II. Bulk samples cooled to the homogeneous nucleation limit," J. Chem. Phys. **87**, 4840–4845 (1987).
[108]J. R. Espinosa, E. Sanz, C. Valeriani, and C. Vega, "On fluid-solid direct coexistence simulations: The pseudo-hard sphere model," J. Chem. Phys. **139**, 144502 (2013).
[109]E. G. Noya, C. Vega, and E. de Miguel, "Determination of the melting point of hard spheres from direct coexistence simulation methods," J. Chem. Phys. **128**, 154507 (2008).
[110]M. M. Conde, M. A. Gonzalez, J. L. F. Abascal, and C. Vega, "Determining the phase diagram of water from direct coexistence simulations: The phase diagram of the TIP4P/2005 model revisited," J. Chem. Phys. **139**(15), 154505 (2013).
[111]V. C. Weiss, M. Rullich, C. Köhler, and T. Frauenheim, "Kinetic aspects of the thermostatted growth of ice from supercooled water in simulations," J. Chem. Phys. **135**(3), 034701 (2011).
[112]J. Y. Yan and G. N. Patey, "Molecular dynamics simulations of ice nucleation by electric fields," J. Phys. Chem. A **116**(26), 7057–7064 (2012).
[113]P. Montero de Hijes, J. Espinosa, C. Vega, and E. Sanz, "Ice growth rate: Temperature dependence and effect of heat dissipation," J. Chem. Phys. **151**(4), 044509 (2019).
[114]D. Frenkel and A. J. Ladd, "New Monte Carlo method to compute the free energy of arbitrary solids. Application to the fcc and hcp phases of hard spheres," J. Chem. Phys. **81**(7), 3188–3193 (1984).
[115]J. M. Polson, E. Trizac, S. Pronk, and D. Frenkel, "Finite-size corrections to the free energies of crystalline solids," J. Chem. Phys. **112**(12), 5339–5342 (2000).
[116]C. Vega, E. Sanz, J. L. F. Abascal, and E. G. Noya, "Determination of phase diagrams via computer simulation: Methodology and applications to water, electrolytes and proteins," J. Phys.: Condens. Matter **20**(15), 153101 (2008).
[117]C. Vega and J. L. F. Abascal, "Relation between the melting temperature and the temperature of maximum density for the most common models of water," J. Chem. Phys. **123**, 144504 (2005).
[118]R. Shi and H. Tanaka, "Microscopic structural descriptor of liquid water," J. Chem. Phys. **148**, 124503 (2018).
[119]M. J. Cuthbertson and P. H. Poole, "Mixturelike behavior near a liquid-liquid phase transition in simulations of supercooled water," Phys. Rev. Lett. **106**, 115706 (2011).
[120]Z. Yu, R. Shi, and H. Tanaka, "A unified description of the liquid structure, static and dynamic anomalies, and criticality of TIP4P/2005 water by a hierarchical two-state model," J. Phys. Chem. B **127**, 3452–3462 (2023).
[121]G. A. Appignanesi, J. A. Rodriguez Fris, and F. Sciortino, "Evidence of a two-state picture for supercooled water and its connections with glassy dynamics," Eur. Phys. J. E **29**, 305–310 (2009).
[122]E. Duboué-Dijon and D. Laage, "Characterization of the local structure in liquid water by various order parameters," J. Phys. Chem. B **119**(26), 8406–8418 (2015).
[123]F. Caupin and M. A. Anisimov, "Minimal microscopic model for liquid polyamorphism and waterlike anomalies," Phys. Rev. Lett. **127**(18), 185701 (2021).
[124]S. V. Buldyrev, T. J. Longo, F. Caupin, and M. A. Anisimov, "Monte Carlo simulations of the blinking-checkers model for polyamorphic fluids," Mol. Phys. **122**(21–22), e2371555 (2024).
[125]J. Russo, F. Leoni, F. Martelli, and F. Sciortino, "The physics of empty liquids: From patchy particles to water," Rep. Prog. Phys. **85**(1), 016601 (2022).
[126]M. Sprik and M. L. Klein, "A polarizable model for water using distributed charge sites," J. Chem. Phys. **89**(12), 7556–7560 (1988).
[127]U. Niesar, G. Corongiu, E. Clementi, G. Kneller, and D. Bhattacharya, "Molecular dynamics simulations of liquid water using the NCC ab initio potential," J. Phys. Chem. **94**(20), 7949–7956 (1990).
[128]J. Brodholt, M. Sampoli, and R. Vallauri, "Parameterizing a polarizable intermolecular potential for water," Mol. Phys. **86**(1), 149–158 (1995).
[129]G. N. Patey, G. M. Torrie, and J. P. Valleau, "A Monte Carlo study of the dense polarizable dipolar hard sphere fluid," J. Chem. Phys. **71**(1), 96–103 (1979).
[130]O. Demerdash, L.-P. Wang, and T. Head-Gordon, "Advanced models for water simulations," Wiley Interdiscip. Rev.: Comput. Mol. Sci. **8**(1), e1355 (2018).
[131]C. H. Pham, S. K. Reddy, K. Chen, C. Knight, and F. Paesani, "Many-body interactions in ice," J. Chem. Theory Comput. **13**(4), 1778–1784 (2017).
[132]E. Lambros and F. Paesani, "How good are polarizable and flexible models for water: Insights from a many-body perspective," J. Chem. Phys. **153**(6), 060901 (2020).
[133]M. S. Daw, S. M. Foiles, and M. I. Baskes, "The embedded-atom method: A review of theory and applications," Mater. Sci. Rep. **9**(7–8), 251–310 (1993).
[134]A. R. Tejedor, I. Sanchez-Burgos, M. Estevez-Espinosa, A. Garaizar, R. Collepardo-Guevara, J. Ramirez, and J. R. Espinosa, "Protein structural transitions critically transform the network connectivity and viscoelasticity of RNA-binding protein condensates but RNA can prevent it," Nat. Commun. **13**(1), 5717 (2022).